

Strange Hadron Resonances: Freeze-Out Probes in Heavy-Ion Collisions

C. Markert*, G. Torrieri[†] and J. Rafelski[†]

**Yale University, New Haven, Connecticut 06520*

[†]Department of Physics, University of Arizona, Tucson, AZ 85721

Abstract. Hyperon resonances are becoming an extremely useful tool allowing the study of the properties of hadronic fireballs made in heavy ion collisions. Their yield, compared to stable particles with the same quark composition, depends on hadronization conditions. The resonance's short lifetime makes them ideal probes of the fireball chemical freeze-out mechanisms. An analysis of resonance abundance in heavy ion collisions should be capable of distinguishing between possible hadronization scenarios, in particular between sudden and gradual hadronization. In this paper, we review the existing SPS and RHIC experimental data on resonance production in heavy ion collisions, and discuss in terms of both thermal and microscopic models the yields of the two observed resonances, K^* and $\Lambda(1520)$. We show how freeze-out properties, namely chemical freeze-out temperature and the lifetime of the interacting hadron phase which follows, can be related to resonance yields. Finally, we apply these methods to SPS and RHIC measurements, discuss the significance and interpretations of our findings, and suggest further measurements which may help in clarifying existing ambiguities.

INTRODUCTION AND MOTIVATION

The experimental measurement of short-lived hadron resonances can potentially be very useful in clarifying some of the least understood aspects of heavy ion collisions. In general, evolution of a hot hadronic system proceeds according to Fig. 1. When mesons and baryons emerge from a pre-hadronic state, presumably quark gluon plasma, their abundances are expected to be fixed by hadronization temperature and chemical fugacities. This stage of fireball evolution is commonly known as chemical freeze-out. After initial hadronization, the system may evolve as an interacting hadron gas. At a certain point (which can vary according to particle species), thermal freeze-out, where hadrons stop interacting, is reached.

A quantitative understanding of the above picture is crucial for any meaningful analysis of the final state particles. Many probes of deconfinement are most sensitive when the dense hadron matter fireball breakup is sudden and re-interaction time short or non-existent. Final state particles could, however also emerge remembering relatively little about their primordial source, having been subject to re-scattering in purely hadronic gas phase. In fact, theoretical arguments have been advanced in support of both a sudden reaction picture [1, 2] and a long re-interaction timescale [3]. Both pictures have been applied to phenomenological fits of hyperon abundances and distributions [4, 5].

It is apparent that hyperon resonances can be crucial in resolving this ambiguity: their initial abundance, compared to stable particles with the same quark composition,

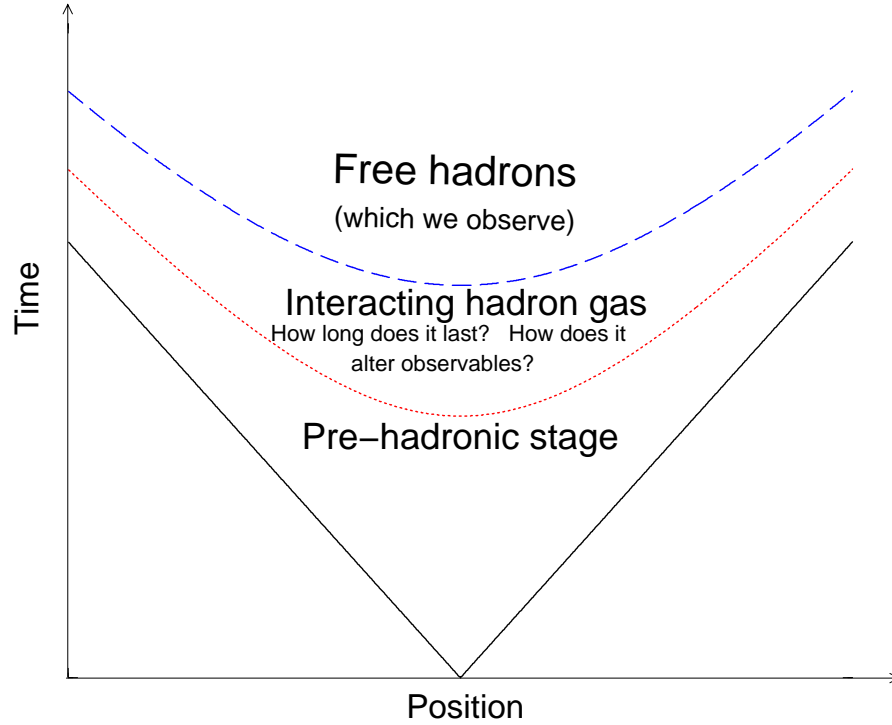


FIGURE 1. Stages of the space-time evolution of a heavy ion collision. At a certain moment in proper time (known as chemical freeze-out), hadrons emerge. The system then evolves as an interacting hadron gas, until thermal freeze-out, the point at which all elastic interactions cease as well.

depends primarily to the temperature at hadron formation. However, the observed abundance will be potentially quite different, and will strongly depend on the lifetime of the interacting hadron gas phase. Resonances can only be observed via invariant mass reconstruction, and their short lifetime means that they can decay within the interacting hadron gas (Fig. 2). In this case, the decay products can undergo re-scattering, and emerge from the fireball with no memory about the parent resonance. Thus, the observable resonance abundance is sensitive to precisely those parameters needed to distinguish between the sudden and gradual freeze-out models.

This paper offers a pedagogical description of what we know about resonance production in heavy ion collisions. We start with a review of presently available experimental data, and the open questions which arise. We then proceed to describe how to calculate the initial resonance abundance and the effect of re-scattering in terms of the hadronization temperature and the lifetime of the interacting hadron gas. We show how these two parameters can be extracted from the experimental observations. Finally, we discuss possible answers to experimental challenges raised in the first section, and suggest ways by which these questions could be resolved by further measurements. This survey incorporates recently published experimental measurements [6, 7, 8, 9, 10] and theoretical results [13, 14, 15].

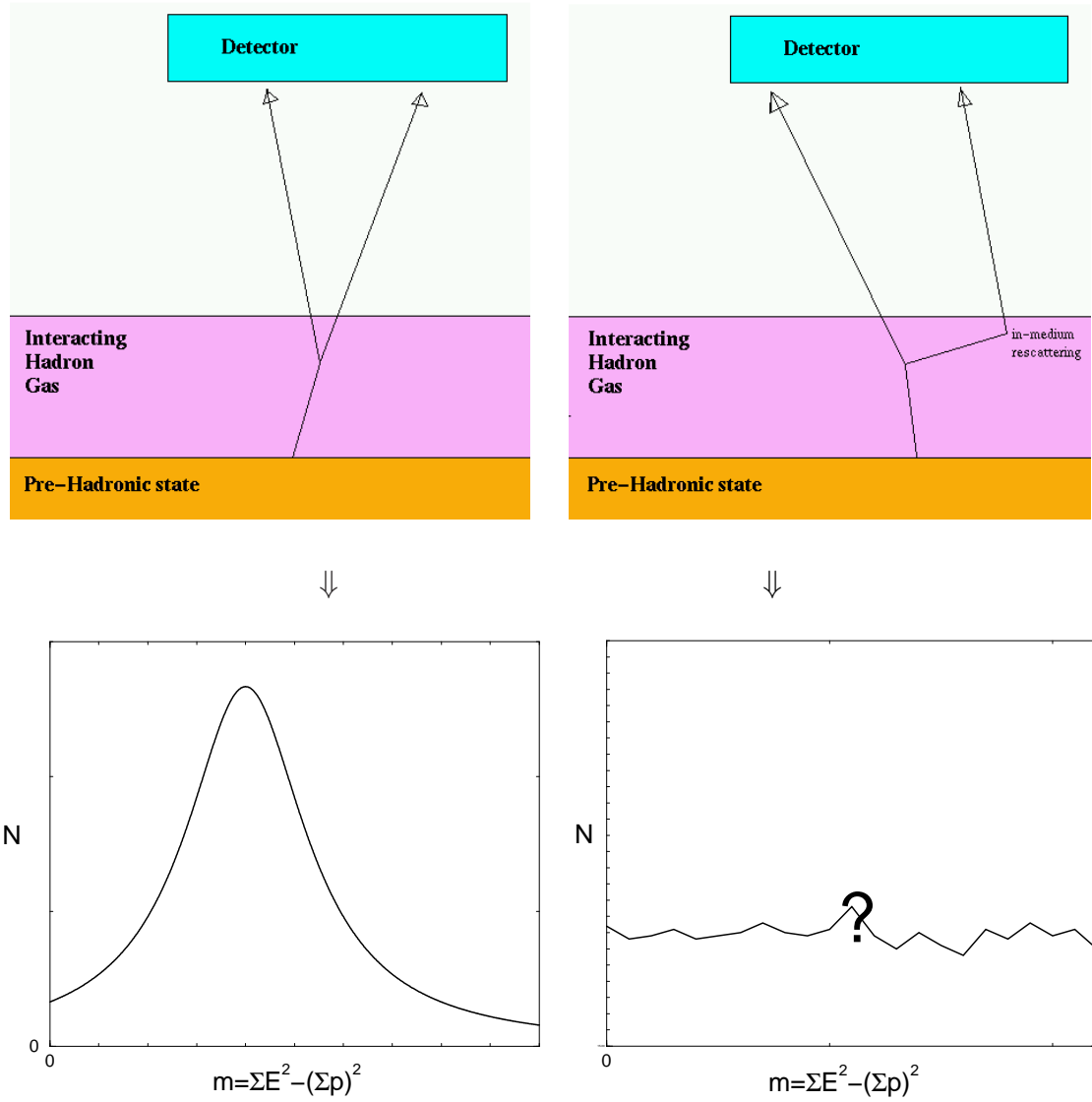


FIGURE 2. Re-scattering can inhibit resonance reconstruction. Left: in case the resonance decay products reach the detector without further interactions, their invariant mass distribution should yield a clear peak at the resonance mass, with the yield corresponding to resonance abundance. Right: should these decay products undergo re-scattering before reaching the detector, the signal may be indistinguishable from the background caused by unrelated particle pairs. Generally a weakening by the medium of the resonance invariant mass signal must be allowed for.

EXPERIMENTAL MEASUREMENTS

Resonance Reconstruction

Resonances are detected through invariant mass reconstruction of their decay products. The channels relevant for the here considered K^{*0} , $\Lambda(1520)$ resonances are:

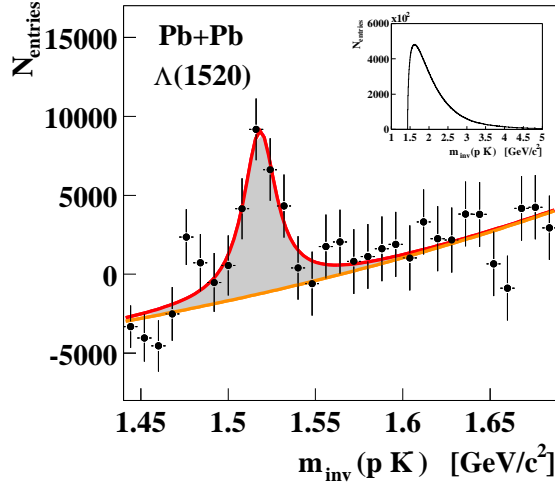


FIGURE 3. $\Lambda(1520)$ mass plot after mixed event background subtraction with a Breit-Wigner fit from NA49 at $\sqrt{s} = 17$ GeV, insert plot: Mass plot before mixed event background subtraction [8].

$$\begin{aligned}\bar{K}^{*0}(892) &\rightarrow \pi^+ + K^-, \\ K^{*0}(892) &\rightarrow \pi^- + K^+, \\ \Lambda(1520) &\rightarrow p + K^-, \end{aligned}$$

and the proposed Σ^* measurement would be performed via the observation of the decay:

$$\Sigma^*(1385) \rightarrow \Lambda + \pi.$$

At present, NA49 reported a $\bar{K}^* \rightarrow K^- \pi^+$ signal [6], while STAR published an average of K^* and \bar{K}^* yields [7].

Both the STAR [16] and the NA49 [17] experiments perform this reconstruction based on data collected in their large volume *Time Projection Chambers* (TPC) detectors. Charged particle momenta are obtained by a measurement of their trajectories in a uniform magnetic field, while particle identification is done evaluating the rate of energy loss dE/dx in the TPC [18]. A centrality trigger selects the 14% (STAR) and 5% (NA49) most central inelastic interactions. The decay daughter candidates are selected via their momenta and dE/dx . The resonance signal is obtained by the invariant mass reconstruction of each pair combination and the subtraction of a mixed event background estimated by combining candidates from different events (Figure 3). The multiplicity is obtained after applying correction factors for acceptance, particle identification cut, reconstruction efficiency and branching ratio.

TABLE 1. Resonance mass and width

collision	Energy GeV	particle	mass MeV/c ²	σ_{mass} MeV/c ²	width MeV/c ²	σ_{width} MeV/c ²	reference
Pb+Pb	17.2	$\Lambda(1520)$	1518.1	2.0	22.7	6.5	[8]
Au+Au	130	K^{*0}	893.0	3.0	58.0	15.0	[10]
Au+Au	130	\overline{K}^{*0}	896.0	4.0	63.0	11.0	[10]
PDG		$\Lambda(1520)$	1519.5	1.0	15.6	0.6	[11]
PDG		K^{*0} and \overline{K}^{*0}	896.1	0.27	50.7	15.0	[11]

Determination of Width and Mass

The measured width and mass of $\Lambda(1520)$ and K^* in heavy ion collisions is in agreement within the statistical errors with the values from the Particle Data Group (table 1).

Within the statistical error there are no width broadening or mass shifts observed. While there is no calculation available that estimates the width and mass profile of a resonance by taking the medium density evolution during the expansion into account, shifts in width and mass would be expected in a lengthy hadron gas phase [19]. A prediction based on relativistic chiral SU(3) dynamic calculations [20, 21] gives a 100 MeV broadening of the $\Lambda(1520)$ resonance and a mass shift of about 100 MeV to lower masses in medium at a density of $\rho = 0.17 \text{ fm}^{-3}$.

The fact that the $\Lambda(1520)$ NA49 signal from Pb+Pb reactions shows no width broadening within the errors, indicates that only the decay products coming from the vacuum $\Lambda(1520)$ decay are observed. Any medium modified $\Lambda(1520)$ resonances must thus decay rapidly within the medium, with decay products rescattering, or, alternatively no such $\Lambda(1520)$ -medium interaction is present. To distinguish these alternatives one needs to consider the yields of $\Lambda(1520)$.

Particle Multiplicities

Experimental results for K^* and $\Lambda(1520)$ resonance production in heavy ion collisions are available from NA49 experiment in central Pb+Pb and p+p at $\sqrt{s} = 17 \text{ GeV}$ and from STAR experiment in central Au+Au $\sqrt{s_{\text{NN}}} = 130 \text{ GeV}$ collision energy and are shown in table 2.

Comparing $\Lambda(1520) \rightarrow pK$ yields at different experiments, we see a marked decrease from elementary p+p to Pb+Pb collisions at 17.2 GeV, which is even more pronounced in the $\Lambda(1520)/\Lambda$ ratio (figure 4 left and right). This suggests that heavy ion collisions are not merely superpositions of elementary p+p collisions. Here we can ask the first question. "Why is the $\Lambda(1520)$ signal from the invariant mass reconstruction in the K-p decay channel actually suppressed in heavy ion collisions, whereas all other hyperons are enhanced?" Moreover, the K^* over π production at the same energy indicates no such signal decrease from p+p to Pb+Pb collisions, shown in figure 5. The second question is

TABLE 2. Resonance yields

collision	Energy GeV	particle	yield	reference
p+p	17.2	$\Lambda(1520)$	0.0121 ± 0.003	[6, 8]
p+Pb	17.2	$\Lambda(1520)$	0.0072 ± 0.003	[6]
Pb+Pb	17.2	$\Lambda(1520)$	1.45 ± 0.40	[6, 8]
Pb+Pb	17.2	K^* 5-10% most central	12.88 ± 4.53	[6]
Au+Au	130	K^* $(dN/dy)_{y< 0.5 }$	10.0 ± 0.8	[10, 7]
Au+Au	130	$\Lambda(1520)$	$< 4.2^*$	[9]

* at 95% confidence level

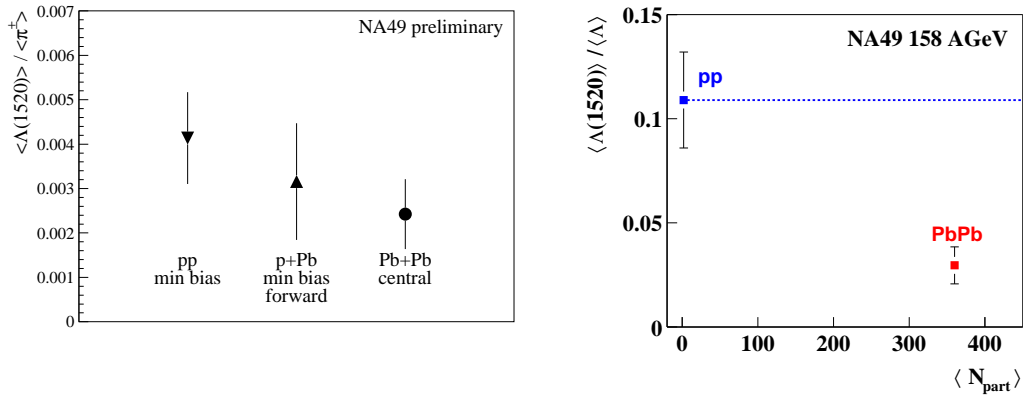


FIGURE 4. Left: $\Lambda(1520)/\pi^+$ as a function of participants for p+p, p+Pb and Pb+Pb collisions at 158 AGeV [6]. Right: $\langle \Lambda(1520) \rangle / \langle \Lambda \rangle$ ratio as a function of number of participants. Data points are p+p and central Pb+Pb collisions from NA49.

now "Why is no comparable suppression observed in the K^* ?" A hint for the signal loss could be due to secondary interactions is the measurement of the $\Lambda(1520)$ production in p+Pb collisions which seems to be decreasing. However the errors are too large to say this conclusively (figure 4 left).

For the collision energy of $\sqrt{s_{NN}} = 130$ GeV there is only an upper limit for the $\Lambda(1520)$, namely 4.2 at 95% confidence level (2σ). The expected multiplicity from extrapolated elementary p+p reactions including an addition factor of 2 for strangeness enhancement (taken from Λ at SPS [22]) is ~ 7.7 . The upper limit estimate indicates that we see at RHIC energies the same trend of signal loss as at SPS energies. The K^*/K ratio at RHIC energies fits in within errors to the ratios from elementary p+p and e^+e^- collisions figure 6, that leads us to the conclusion that there is no indication of K^* signal loss related to K yield. Our conclusions from the results from SPS and RHIC energies are in agreement.

A recent UrQMD calculation [33] predicts for the K^* a signal loss of 66 % and for the $\Lambda(1520)$ 50 % at SPS energies due to re-scattering of the decay products (figure 7). At RHIC energies the signal loss is on the order of 55% for K^* and 30 % for $\Lambda(1520)$ [34]. The K^* yield at A+A collisions for SPS and RHIC energies shows no indication

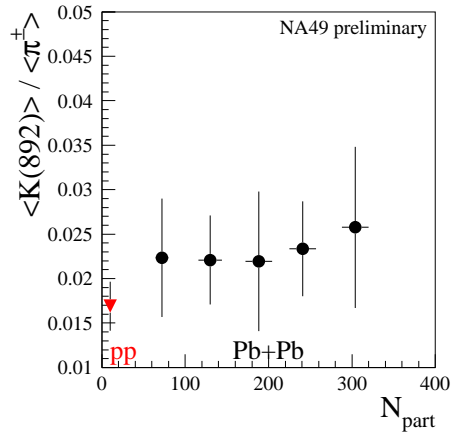


FIGURE 5. $K^*(892)/\pi$ as a function of participants for p+p and Pb+Pb collisions at 158 AGeV.

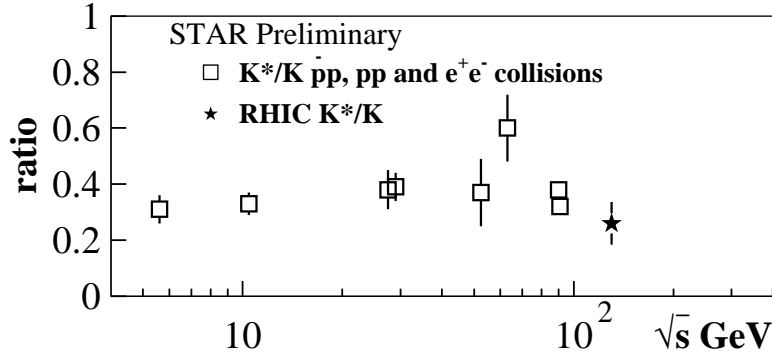


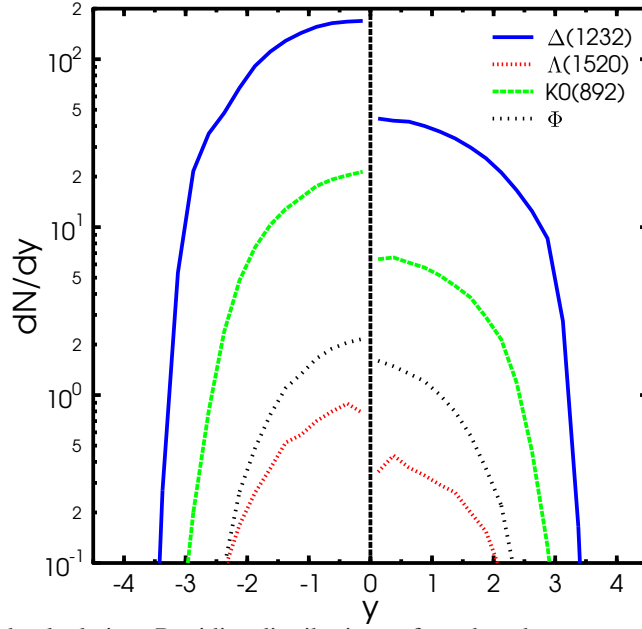
FIGURE 6. K^{*0}/K measured in different colliding systems at different energies. For elementary e^+e^- and pp collisions in comparison [23, 24, 25, 26, 27, 28, 30, 31, 32] with the heavy ion collision Au+Au at RHIC energies $\sqrt{s_{NN}} = 130$ GeV [7].

of signal loss and therefore it is not in agreement with the predicted signal loss from the UrQMD model. This means that the mechanism of re-scattering alone can not explain the signal loss of the $\Lambda(1520)$ with respect to the K^* production.

As table 3 shows, the agreement of the data with thermal model predictions presents a considerable problem as well. At SPS energies, thermal model calculations over-predict the $\Lambda(1520)$ yield by a factor of two [36], while the upper limit measurement of $\Lambda(1520)$ from STAR is 30% lower than the predicted value. However, published thermal model-calculations significantly under-predict the K^* (although, as will be seen in the next section, the observed K^* is consistent with thermal production at a lower freezeout temperature).

TABLE 3. Particle yields from thermal model predictions

collision	Energy GeV	particle	predicted yield	reference
Pb+Pb	17.2	$\Lambda(1520)$	3.48	[35]
Pb+Pb	17.2	$\Lambda(1520)$	5.20	[3]
Au+Au	130	K^*/h^-	0.037	[12]

**FIGURE 7.** Urqmd calculation. Rapidity distributions of produced resonances (left half), and of the resonances which remain observable after thermal freezeout[33].

MODELING RESONANCES IN HEAVY ION COLLISIONS

Direct production at hadronization

We assume that at hadronization, a volume element will be at thermal and chemical equilibrium in its local rest frame. This means hadrons produced directly from a medium at temperature T (much lower than the particle mass, as in all cases considered here) fill the available phase space according to the relativistic Boltzmann distribution:

$$dN \propto g d^3p f(\lambda, E, T), \quad (1)$$

$$f(\lambda, E, T) = \lambda e^{-E/T}. \quad (2)$$

Here g is the statistical degeneracy and $\lambda = e^{\mu/T}$ is the hadron's fugacity. Since a hadron is a composite state of flavored quarks, it is natural to parametrize its fugacity as a product of the flavor fugacities of each constituent. As a further step, each quark's fugacity can be decomposed into a term λ_i controlling the net flavor ($q - \bar{q}$) and an

occupancy number γ_i which determines the number of quark-antiquark pairs. Therefore,

$$\lambda = \prod_{q=1}^n \lambda_i \gamma_i, \quad (3)$$

$$\lambda_q = \lambda_{\bar{q}}^{-1}, \quad (4)$$

$$\gamma_q = \gamma_{\bar{q}}, \quad (5)$$

and the precise values of λ_i, γ_i can be determined from global particle abundance fits [2].

We can now change to rapidity (y) and transverse mass (m_T) coordinate system, where transverse and longitudinal directions are defined with respect to the beam. (The advantage of this system is that m_T is invariant between the lab and the center of mass frames, while the rapidity transforms additively).

$$dN = gm_T^2 \cosh(y) dm_T dy f(\lambda, m_T \cosh(y), T) \quad (6)$$

$$m_T = \sqrt{m^2 + p_T^2} \quad (7)$$

$$y = \frac{1}{2} \ln \left(\frac{E + p_L}{E - p_L} \right) \quad (8)$$

To get particle ratios in a certain region of phase space collective expansion (flow) as well as freeze-out geometry has to be included. The most general way to do this is to introduce a space-time hypersurface (a 3-D surface in 4-D space-time) $d\Sigma_\mu$, which will transform as a 4-vector. This vector can either be time-like, corresponding to a freeze-out surface evolving in time, or space-like, corresponding to a freeze-out occurring simultaneously across the fireball volume. The total number of emitted particles will then be

$$N_i = \int d\Sigma_\mu(x) j^\mu(x). \quad (9)$$

We can describe the current 4-vector j^μ in terms of the hadron density in the volume element at rest, (see Eq. 1)

$$j^\mu = n_{\text{rest}} u^\mu = f(\lambda, E_{\text{local}}, T) \frac{p^\mu}{E}, \quad (10)$$

where E_{local} is the energy in the local rest frame with respect to flow, and u^μ is the volume element's 4-velocity.

In the limit of a homogeneous fireball (Temperature and chemical potential constant in space) and full phase space, the total number of produced particles is, as expected, independent of flow and hadronization geometry, since in this case Eq. (9) becomes

$$N = \int d\Sigma_\mu(x) j^\mu(x) = \int d\Sigma_\mu(x) u^\mu(x) \int d^3p f(\lambda, E_{\text{local}}, T) = V \int d^3p f(\lambda, E_{\text{local}}, T). \quad (11)$$

We can now find N analytically

$$N = V \lambda \int d^3p e^{-(p^2 + m^2)/T} = \frac{1}{2\pi^2} \lambda m^2 T K_2(m/T) \quad (12)$$

remembering the properties of Bessel functions

$$K_n(x) = \frac{2^n n!}{(2n)!} x^{-n} \int_0^\infty dz (z^2 + x^2)^{-\frac{1}{2}} z^{2n} e^{-\sqrt{z^2 + x^2}}, \quad (13)$$

If the fireball is not homogeneous, or we want to only calculate the yield within the experimental acceptance limits, we need to use a more general result. Putting Eqs. (9) and (10) together one gets the relativistically invariant Cooper-Frye formula [40]

$$E \frac{d^3 N}{d^3 p} = \frac{1}{2\pi m_T} \frac{dN}{dy m_T} = \int d\Sigma_\mu p^\mu f(\lambda, p_\mu u^\mu, T) \theta(\Sigma_\mu p^\mu), \quad (14)$$

where the step function $\theta(\Sigma_\mu p^\mu)$ has been introduced to eliminate unphysical emission in the direction opposite to expansion [41, 42]. Eq. (14) can be integrated to yield the total particle number over an arbitrary phase space region

$$N = \int \frac{d^3 p}{E} \int d\Sigma_\mu p^\mu f(\lambda, p_\mu u^\mu, T) \theta(\Sigma_\mu p^\mu) \quad (15)$$

Many of the parameters used in these formulae can be eliminated by judicious choice of observables. For instance, the ratio of a hyperon resonance to its ground state is independent of the chemical potential, since all chemical potential terms cancel out. Suitable ratios include Σ^*/Λ , $\Lambda(1520)/\Lambda$, K^{*0}/K^+ , \bar{K}^{*0}/K^- . A particular case is the K^0/\bar{K}^0 system: While the K^{*0} decays long before it has a chance of oscillate, the experimentally observed K_S is a superposition of K^0 and \bar{K}^0 . Suitable average are \bar{K}^{*0}/K^- (measured by NA49 [6]) K^{*0}/K^+ and $(K^* + \bar{K}^*)/(K^+ + K^-)$ (measured by STAR [7]).

Moreover, we found that for these ratios (more generally for ratios of particles with comparable masses), effects due to flow and surface geometry cancel out to a very good approximation and Eq. (12) gives the produced particle ratios to a good accuracy.

Feed down from resonance decays

Many of the hyperons considered here can be produced either directly at hadronization or in the decay of a resonance produced earlier. For instance,

$$\frac{\Lambda(1520)}{\Lambda_{\text{total}}} = \frac{\Lambda(1520)}{\Lambda + (\Sigma^0 \rightarrow \Lambda \gamma) + (\Sigma^* \rightarrow \Lambda \pi) + (\Sigma^* \rightarrow \Sigma^0 \pi \rightarrow \Lambda \pi \gamma)}. \quad (16)$$

Unless a resonance will be directly reconstructed by the experiment, its decay products will be a component in the hyperon abundances (albeit with a subtly different momentum distribution). This contribution, therefore, will need to be taken into account through calculation. As in the case of direct production, all kinematic effects are integrated out in a calculation of the total yield, and one simply sums each term in the resonance contribution as a term of the form given in Eq. (12). If a finite acceptance in phase space

needs to be taken into account, however, a distribution of decay products will need to be computed from the statistical distribution of resonances.

We assume that, in a decay of the form,

$$R \rightarrow 1 + 2 + \dots, \quad (17)$$

any dynamical effects in the decay (the S-matrix) average out over a statistical sample of many resonances. In other words, in the rest frame comoving with the “average” resonance, the distribution of the decay products will be isotropic. The rate of particles of type 1 (as in Eq. (17)) produced with momentum \vec{p}_1^* in the frame at rest w.r.t. the resonance will then simply be given by the Lorentz-Invariant phase space factor of a particle of mass M_1 and momentum \vec{p}_1^* within a system with center of mass energy equal to the resonance mass M_R .

$$\frac{d^3 N_1}{d^3 p_1^*} = b \int \prod_{i=2}^n \frac{d^3 p_i^*}{2E_i^*} \delta\left(\sum_{i=2}^N p_i^* - p_1^*\right) \delta\left(\sum_{i=2}^N E_i^* - E_1^* - M_R\right), \quad (18)$$

where b is the branching ratio of the considered decay channel. All that is left is to change coordinates from the resonance’s rest frame (p^*, E^*) to the lab frame (p, E) .

If more than two bodies are considered, this calculation becomes more involved [45]. For the general N-body case, it is better left to Monte Carlo methods [46]. In the case of the 2-body decay, the situation is greatly simplified by the fact that p^*, E^* are fixed by energy-momentum conservation to,

$$E_1^* = \frac{1}{2M_R}(M_R^2 - m_1^2 - m_2^2), \quad (19)$$

$$p_1^* = -p_2^* = \sqrt{E_1^{*2} - m_1^2}. \quad (20)$$

Putting the constraints in Eq. (19) into Eq. (18) one gets, after some algebra [44]

$$\frac{dN}{dm_{T1}^2 dy_1} = \frac{b}{4\pi p_1^*} \int_{Y-}^{Y+} dY_1 \int_{M_T-}^{M_T+} dM_{T1}^2 J \frac{d^2 N_R}{dM_{TR}^2 dY_R}, \quad (21)$$

$$J = \frac{M_R}{\sqrt{P_{TR}^2 p_{T1}^2 - (M_R E_R^* - M_{TR} m_{T1} \cosh \Delta Y)^2}}, \quad (22)$$

$$\Delta Y = Y_R - y_1. \quad (23)$$

J is simply the Jacobian of the transformation from the resonance rest frame to the lab frame, and the limits of the kinematically allowed integration region are:

$$Y_{\pm} = y_1 \pm \sinh^{-1} \left(\frac{p_1^*}{m_{T1}} \right),$$

$$M_T^{\pm} = M_R \frac{E_R^* m_{T1} \cosh(\Delta Y) \pm p_{T1} \sqrt{p_1^{*2} - m_{T1}^2} \sinh^2(\Delta Y)}{m_{T1}^2 \sinh^2(\Delta Y) + m_1^2}.$$

TABLE 4. Resonances contributing to Λ and K production, with their degeneracies, rest-frame momentum (p^*) and possibility for experimental reconstruction

g	Reaction	p^* MeV	branching	visible?
≈ 4	$\Sigma^{*0}(1385) \rightarrow \Sigma^0 \pi^0$	127	$\approx 4\%$	No
8	$\Sigma^{*\pm}(1385) \rightarrow \Lambda \pi^\pm$	208	88%	Yes
4	$\Sigma^{*0}(1385) \rightarrow \Lambda \pi^0$	208	88%	No
2	$\Sigma^0 \rightarrow \Lambda \gamma$	74	100%	No
4	$\Lambda(1520) \rightarrow N \bar{K}$	244	45%	Yes
3	$K^{*0}(892) \rightarrow K^+ \pi^-$	291	67%	Yes

We now apply the methods outlined here to calculate ratios at hadronization for a range of experimentally observable resonances, both at full and central rapidity ($|y| \leq 0.5$). The total ratio was calculated using the analytical formula in Eq. (12), while for mid-rapidity equations in Eq. (15) and (21) were used. In the midrapidity calculation we used a uniform spherically symmetric expanding fireball, with a hadronization surface used earlier by fits in [5] and [44],

$$d\Sigma_\mu = (1, -\frac{\partial t_f}{\partial r} \vec{e}_r) d^3\vec{r}, \quad (24)$$

where \vec{e}_r is the unit vector in the radial direction and $\partial t_f / \partial r$ is a constant. We mentioned earlier that flow and hadronization surface details cancel out to a very good approximation when hadron masses are comparable. In fact, when we varied $\partial t_f / \partial r$, the results did not change by more than a percentage point. Table 4 summarizes the decay processes considered in our analysis and their parameters (Clebsch-Gordon coefficients have been used to estimate decays such as $(N^{*0} \rightarrow N^+ \pi^-) / (N^{*0} \rightarrow N^0 \pi^0)$).

In Fig. 8 we show the relative thermal production ratios at chemical freeze-out over the entire spectrum of rapidity and m_T (solid lines) and central rapidity range (dashed lines). The sensitivity of resonance yields to hadronization temperature is apparent for all resonances under consideration. In particular, the Σ^* emerges as a very promising candidate for further study. For example, at the lowest current estimates ($T \simeq 100$ MeV) of the final break up temperature in 158A GeV SPS collisions 33% of Λ are arising from primary Σ^* , the percentage rises to slightly more than 50% if chemical freeze-out occurs at $T = 190$ MeV. Both SPS and STAR detectors are capable to measure hyperon and resonance yields well within the precision required to distinguish between the two limiting cases.

as we discussed earlier, the experimentally observed K^* yield is compatible with the thermally produced ratio for a range of hadronization temperatures, but the $\Lambda(1520)$ seems very suppressed. To discuss this further, an estimation of the effect of rescattering on resonance abundances is necessary.

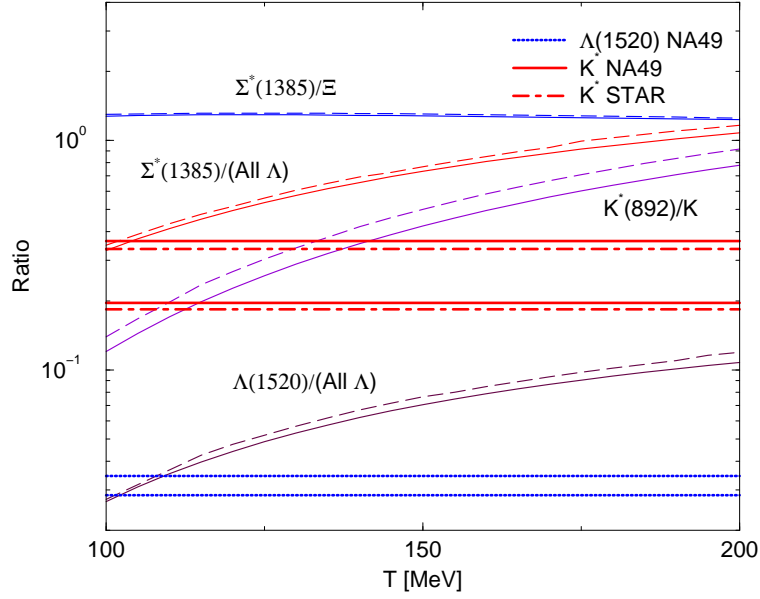


FIGURE 8. Temperature dependence of ratios of Σ^* , K^{*0} and $\Lambda(1520)$ to the total number of observed K Λ s and Ξ s. Branching ratios are included. Dashed lines show the result for a measurement at central rapidity $\Delta y = \pm 0.5$. The experimental measurements (horizontal lines, not Σ^*/Ξ) included in the diagram were presented in the first part of this paper. For the Ξ yields in the diagram, chemical potentials were taken from [2]. It should be noted that the K^*/K ratio is actually \bar{K}^*/K^- for the NA49 measurement, and an average $(K^* + \bar{K}^*)/(K^+ + K^-)$ for STAR.

RESCATTERING

As explained in the introduction, direct observation of resonances relies on invariant mass reconstruction. Therefore, to calculate the observed resonance abundances, rescattering after hadronization will have to be taken into account. This can be looked at within a microscopic model of hadronic matter such as uRQMD. As we have shown earlier, uRQMD failed to describe experimental data if a long re-interaction period and initial thermal model yields were assumed. However, as yet there was no detailed study of the dependence of the resonance yields on the lifetime of the interacting hadron gas phase (the interval between chemical and thermal freeze-out) as well as the chemical freeze-out temperature.

Here, we present such a study using a “back of the envelope” model which nevertheless seems to provide an acceptable qualitative description of the propagation of resonances and their decay products through opaque matter.

We first note in Fig. 8, that the relative Σ^*/Ξ signal is remarkably independent (within 5%) of Temperature. This is because the $\Xi^*(1530)$ contribution cancels nearly exactly the thermal suppression of the Ξ originating in the $\Xi - \Sigma^*$ mass difference. This effect could be used for a direct estimate of the Σ^* lost through rescattering, even without knowledge of the freeze-out temperature, should the chemical parameters (λ_i and γ_i) be independently known. A simple test of sudden hadronization model consists in measurement of the ratio Σ^*/Ξ . If it is significantly smaller than unity, we should expect

a re-equilibration mechanism to be present. Otherwise sudden hadronization probably applies, since Σ^* emerge from chemical freeze-out without undergoing interactions.

We can, however, go further and use the suppression of the considered resonances as a tool capable of yielding a quantitative estimate of the lifetime of the interacting hadron gas phase. We consider the decay of a generic resonance Y^*

$$Y^* \rightarrow Y\pi, \quad (25)$$

in a gas of pions and nucleons. We shall assume that one interaction of either Y or π is sufficient for that resonance to be undetectable, and that the decay products travel through the medium with speed v_i (where i can mean either Y or π). The interaction probability is proportional to v_i , the interaction cross-section of the decay product with each particle in the hadronic medium ($\sigma_{ij}(v_i)$, where j can refer to either pions, Kaons, nucleons or antinucleons. Note that the cross-section itself depends, in a generally complicated way, on the incident momentum, and hence on v_i , and the particle density in the fireball ρ_j . ρ_j is increased by a factor $\gamma_i = 1/\sqrt{1-v_i^2}$ due to Lorentz-contraction, and decreases as time passes because of the fireball's collective expansion (parametrized by the flow velocity v_{flow} , assumed to be of the order of the relativistic sound speed $c/\sqrt{3}$.) The time dependence of the densities will therefore be,

$$\rho_j(t) = \gamma_i \rho_{0j} \left(\frac{R}{R + v_{\text{flow}} t} \right)^3, \quad (26)$$

and ρ_{0j} , the density of j at hadronization, can be calculated from the chemical freeze-out temperatures and chemical potentials. Putting everything together, the rescattering reaction rate is

$$P_i = \sum_{v_i} \left[\sigma_{i\pi}(v_i) \rho_{0\pi} + \sigma_{iK}(v_i) \rho_{0K} + \sigma_{iN}(v_i) \rho_{0N} + \sigma_{i\bar{N}}(v_i) \rho_{0\bar{N}} \right] (\gamma v)_i \left(\frac{R}{R + v_{\text{flow}} t} \right)^3, \quad (27)$$

If we use the average,

$$\sum_{v_i} \sigma(v_i) v_i \gamma_i \simeq \langle \sigma \rangle \langle \gamma v_i \rangle = \langle \sigma \rangle \frac{p_i}{m_i}, \quad (28)$$

(where p and m are the resonance's momentum and mass) Eq. (27) becomes,

$$P_i = \left[\langle \sigma_{i\pi} \rangle \rho_{0\pi} + \langle \sigma_{iK} \rangle \rho_{0K} + \langle \sigma_{iN} \rangle \rho_{0N} + \langle \sigma_{i\bar{N}} \rangle \rho_{0\bar{N}} \right] \frac{p_i}{m_i} \left(\frac{R}{R + v_{\text{flow}} t} \right)^3, \quad (29)$$

Neglecting in-medium resonance regeneration and particle escape from the fireball, the population equation describing the scattering loss abundance (N_i) is:

$$\frac{dN_i}{dt} = \frac{1}{\tau} N_{N^*} - N_i P_i, \quad i = 1, 2 \quad (30)$$

$$\frac{dN_{N^*}}{dt} = -\frac{1}{\tau} N_{N^*} \quad (31)$$

TABLE 5. Scattering model parameters

$\sigma_{\pi N}$ (mb)	σ_{KN}	$\sigma_{\pi\pi}$	$\sigma_{\pi K}$	σ_{NN}	$\sigma_{\bar{N}N}$
24	20	40	20	24	50
Γ_{Σ^*}		$\Gamma_{\Lambda(1520)}$		$\Gamma_{K^{*0}(892)}$	
35 MeV		15.6 MeV		50 MeV	
escape rate (fm ⁻³)			negligible		
v			0.5		
R(fm)			8.145/T [MeV]		
μ_b			220 MeV		

The required nucleon and antinucleon density at hadronization, ρ_{0N} is obtained through Eq. (12)

$$\rho_{0N} = \frac{g}{(2\pi\hbar c)^3} 4\pi m^2 (\lambda_q \gamma_q)^3 T K_2\left(\frac{m}{T}\right), \quad (32)$$

We consider the nucleons to have a mass of $\simeq 1$ GeV, and a degeneracy of six, to take the p,n and the thermally suppressed but higher degeneracy Δ contributions into account. the pion density at hadronization is computed in the massless particle limit, leading to

$$\rho_{0\pi} = \frac{\pi^2}{90} T^3, \quad (33)$$

The model presented here is remarkably insensitive to the individual cross-sectional areas. The values we used in the calculation are given in table 5, but order-of-magnitude variations of the more uncertain cross-sections did not produce variations of more than 30%. Similarly, the value of the initial fireball radius R_0 (which is constrained by the entropy per baryon) does not significantly affect the final ratios. This reassures us that had we used a more exact approach than the approximations in Eq. (28), the qualitative features of our model would not have changed. The results, however, exhibit a very strong dependence on both the Temperature (which fixes the initial resonance yield as well as the hadron density of the fireball) and fireball lifetime (in a short-lived fireball not many resonances decay, so their products do not get a chance to rescatter). Figure 9 shows the dependence of the $\Lambda(1520)/\Lambda$, Σ^*/Λ and $K^{*0}(892)/K$ on the temperature and lifetime of the interacting phase. It is clear that, given a determination of the respective signals to a reasonable precision, a qualitative distinction between the high temperature chemical freeze-out scenario followed by a rescattering phase and the low temperature sudden hadronization scenario can be made. We also note that despite the shorter lifetime of the Σ^* and higher pion interaction cross section, more Σ^* decay products should be reconstructible than in the $\Lambda(1520)$ case, at all but the highest temperatures under consideration. This reinforces our proposal that the Σ^* is a very good candidate for further measurement.

Diagrams such as those in Fig. 9 still contain an ambiguity between temperature and lifetime of the interacting hadron gas phase. A low observed ratio can either mean a low

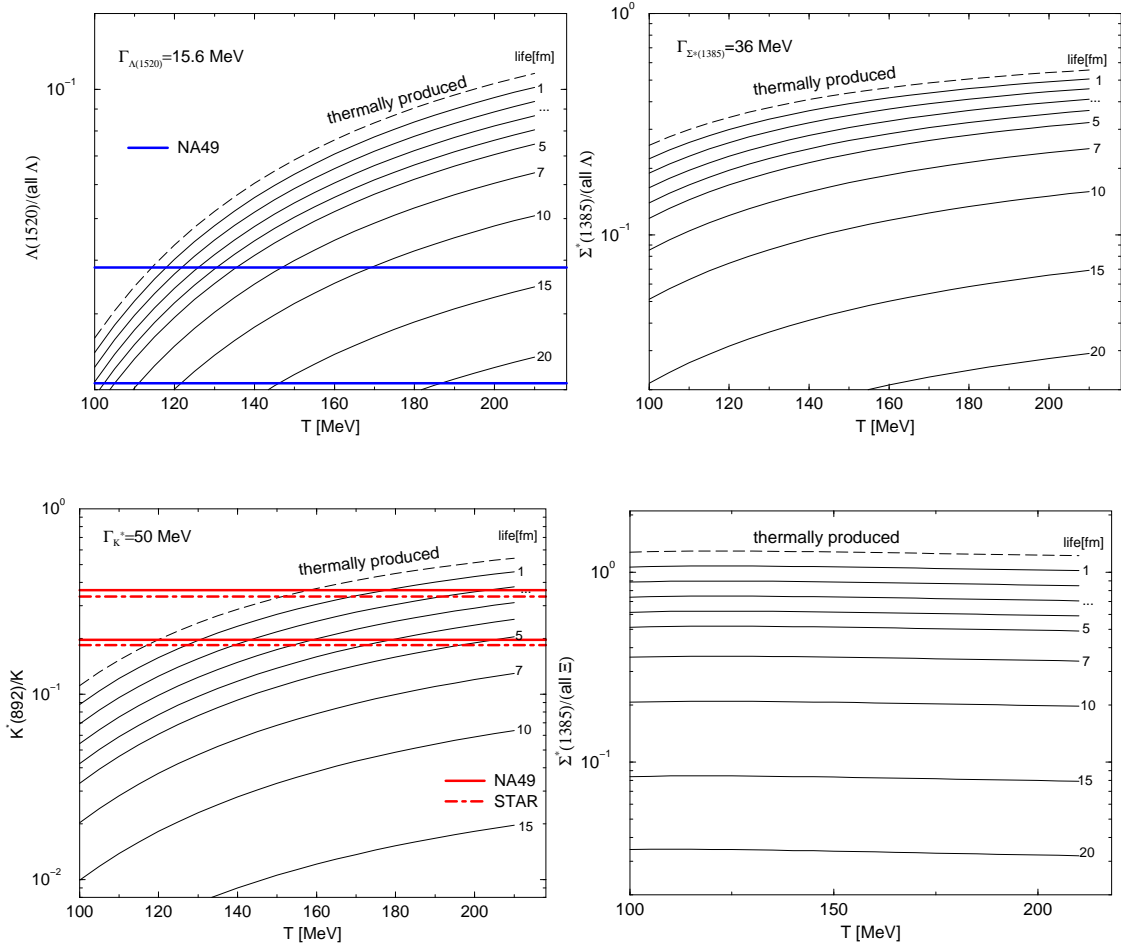


FIGURE 9. Produced (dashed line) and observable (solid lines) ratios $\Lambda(1520)/(\text{total } \Lambda)$, $\Sigma^*/(\text{total } \Lambda)$, K^{*0}/K and $\Xi/(\text{total } \Lambda)$. The solid lines correspond to evolution after chemical freeze-out of 1,2,3,4,5,7,10,15,20 fm/c, respectively. The values at time zero (chemical freezeout) were taken from Fig. 8. See Fig. 8 caption for the meaning of K, K^* .

freeze-out temperature or a lot of rescattering in a long re-interaction phase. However, this ambiguity can be resolved by looking at a selection of resonances, with different masses and lifetimes. Fig. 10 shows how the initial temperature and the lifetime of the re-interaction phase decouple when two resonance ratios are measured simultaneously. A data point on diagrams such as those in Fig. 10 is enough to measure both the hadronization temperature and to distinguish between the sudden freeze-out scenario and a long re-interaction phase. The plots in Fig. 10 can also be used as consistency checks for the model: For example, the near independence of Σ^*/Ξ on temperature means that the equal temperature lines in the Σ^*/Ξ vs Σ^*/Λ diagram are nearly insensitive to the details of the rescattering model. Moreover the mass differences and lifetimes of the Σ^* , K^* combine in such a way as to make the $\Sigma^*/(\text{all } \Lambda)$ vs $K^{*0}(892)/(\text{all } K^-)$ diagram fold into a very narrow band. Any serious shortcoming within our rescattering model would be revealed if the observed particle ratios stray from this band.

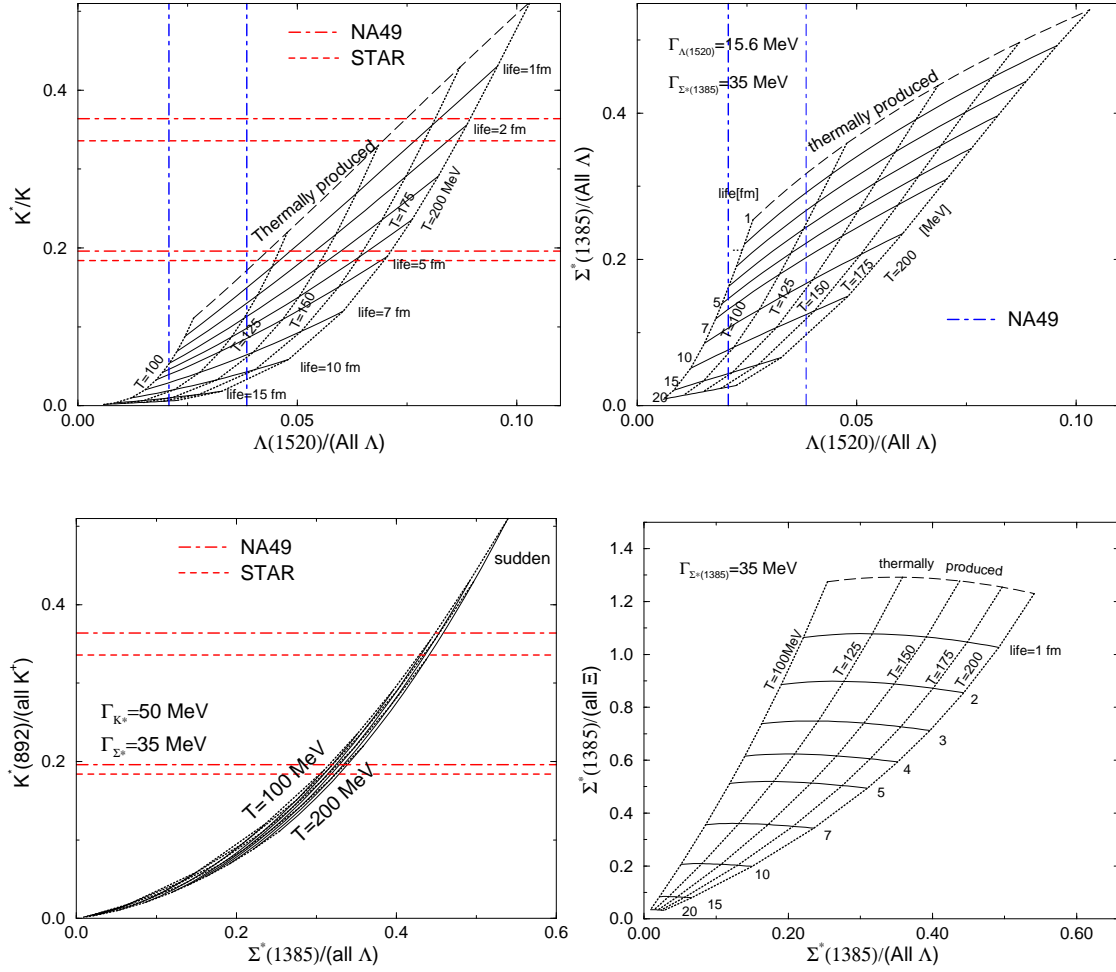


FIGURE 10. How temperature and fireball lifetime decouple when two resonances of different masses and widths are compared. A point on any of the above diagrams is potentially sufficient to fix both of these quantities. The experimental measurements are discussed in the first section. See Fig. 8 caption for the meaning of K, K^* .

DISCUSSION

The first experimental results on short-lived resonances have raised more questions than answers. The low $\Lambda(1520)$ multiplicity measured by NA49, together with its non-detection at STAR, can not be understood with a thermal model exclusively. A $\Lambda(1520)$ suppression factor of at least 2 is needed to reproduce the measured multiplicity. However, this suppression does not appear to result from simple scattering with in-medium particles, described by models such as uRQMD. Such suppression should manifest itself much more strongly in case of the K^* , which has a much shorter lifetime. On the contrary, no comparable depletion has been found in the case of the K^* either at SPS or RHIC energies. Moreover, no broadening of the resonance width, which should accompany a strongly interacting medium, has been observed. If these results are incorporated in the diagrams of Fig. 10, the apparent result is sudden freeze-out with an unphys-

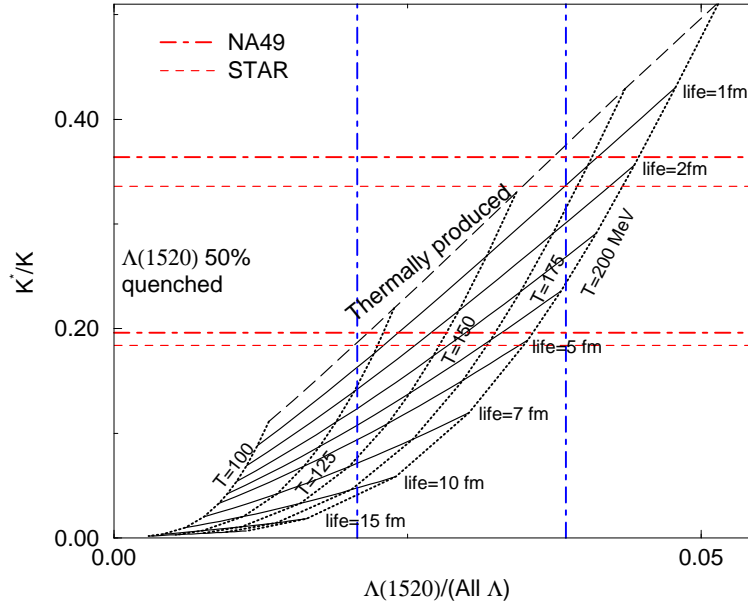


FIGURE 11. K^*/K vs $\Lambda(1520)/\Lambda$ assuming half of the $\Lambda(1520)$ s are suppressed in-medium. See Fig. 8 caption for the meaning of K, K^* .

ically low (~ 100 MeV) temperature. In analysing these results it should be kept in mind that the $\Lambda(1520)$ is a very unusual particle: Unlike most other hadronic resonances ($\Sigma^*, K^*, \Delta, \rho$ ecc.), its high spin is due not to valence quark spin configuration but to the fact that the $\Lambda(1520)$ s valence quarks are believed to be in an $L=1$ state. The greater space separation of $L=1$ wave-functions means that the $\Lambda(1520)$ is especially susceptible to in-medium modifications. As Fig. 11 shows, a 50% suppression of the $\Lambda(1520)$ signal at hadronization would mean the data is perfectly compatible with the sudden freeze-out model described in [1]

Some proposed mechanisms which could lead to a $\Lambda(1520)$ suppression (Some suggested by Berndt Muller at the meeting [49]) are:

- If hadrons form in a quark coalescence process, the $\Lambda(1520)$ would be suppressed for the same reason that $L=1$ (p-shell) electrons are never captured by nuclei [50]: The coalescence probability is dependent on the wave-function overlap at the formed particle's location $\sim |\Psi(x=0)|^2$. The overlap of two particles goes down for higher L states, and is 0 for odd $L=1,3,\dots$ states. However, this effect should also manifest itself in proton-proton collisions, which serve as basis of the AA-reaction yield. We can thus exclude this effect.
- Similarly, the larger spatial extent of the $\Lambda(1520)$ means it is more susceptible to in-medium screening of the strong potential. This mechanism invoked for Charmonium suppression can also suppress states such as the $\Lambda(1520)$.
- In-medium effects can mix the $\Lambda(1520)$ $|S=3/2, I=1/2\rangle$ with the Σ^* $|S=3/2, I=3/2\rangle$ state. Reactions such as

$$\pi + \Lambda(1520) \rightarrow \Sigma^* \quad (34)$$

can deplete the $\Lambda(1520)$ states without a significant effect on the (much more abundant) Σ^* population [14]. This is analogous to the phenomenon of quenching, well known in atomic resonances [51]: Resonance radiation from many gases is known to be suppressed by in-medium collisions, which prevent photon emission by converting the excitation energy of the resonance into kinetic energy.

- Spin-orbit interactions due to in-medium chromomagnetic fields can also mix the $\Lambda(1520)$ with the Σ^* .
- Isospin conservation forbids the decay $\Lambda(1520) \rightarrow \Lambda\pi$ but not $\Lambda(1520) \rightarrow \Lambda\sigma$, which is forbidden in vacuum since $m_\Lambda + m_\sigma > m_{\Lambda(1520)}$. At a temperature high enough for (partial) chiral symmetry restoration to take place, this may no longer be true, and the $\Lambda(1520) \rightarrow \Lambda\sigma$ decay would become possible. In the same way, partial restoration of chiral symmetry may be suppressing the $K^* \rightarrow K\pi$ decay channel.
- Finally, in a long re-interaction phase there is a possibility that the K^* will be re-generated. Processes such as

$$K\pi \rightarrow K^* \rightarrow K\pi$$

will lead to an enhancement of observed K^* . Processes which regenerate the $\Lambda(1520)$, such as

$$pK \rightarrow \Lambda(1520) \rightarrow pK$$

are considerably less likely, due to the suppression of higher ($L > 0$) partial waves.

The last effect can be properly taken into account by a more elaborate rescattering model, which takes all of the microscopic reaction dynamics into account. The other mechanisms are rather complex and uncertain, though for the RHIC system, potential screening, spin-orbit mixing and σ mass change can be explored in a $\mu_B = 0$ lattice calculation. However, these effects also depend on the unusual characteristics of the $\Lambda(1520)$ resonance. It seems to us that all these consideration suggest that other resonances should be studied to constrain the fireball freeze-out properties.

The non-suppression of the K^* makes it likely that other hadron resonances can also be detectable. The diagrams shown in the previous section imply that the Σ^* should be abundantly produced, and it has many characteristics which would make it a logical next step in the study of resonances produced in heavy ion collisions. Other proposed targets of observation are the ρ and even the $\Sigma^0 \rightarrow \Lambda\gamma$.

The sudden freeze-out scenario can be thoroughly tested by the detection of non-strange baryon resonances ($N^*(1440)$ and $\Delta(1230)$). The larger widths of these particles, as well as the larger scattering cross-section in hadronic matter of their decay products, mean that the very detectability of these particles in terms of an invariant mass analysis would be strong evidence of a very fast hadronization process.

ACKNOWLEDGMENTS

Work supported in part by a grant from the U.S. Department of Energy, DE-FG03-95ER40937. Ch. Markert is supported by the Humboldt foundation.

REFERENCES

1. J. Rafelski, J. Letessier *Phys. Rev. Lett.*, **85** (2000) 4695, and references therein.
2. J. Letessier and J. Rafelski, *Int. J. Mod. Phys. E* **9** (2000) 107, and references therein.
3. P. Braun-Munzinger, I. Heppe and J. Stachel, *Phys. Lett. B* **465** (1999) 15.
4. S.V. Akkelin, P. Braun-Munzinger, Yu. M. Sinyukov arXiv:nucl-th/0111050.
5. G. Torrieri and J. Rafelski, *New Jour. Phys.* **3** (2001) 12.
6. V. Friese [NA49 Collaboration], *Nucl. Phys. A* **698** (2002) 487.
7. P. Fachini for the STAR Collaboration, SQM2001, *J. Phys. G* (2002) at press.
8. C. Markert for the NA49 Collaboration, poster presentation at QM2001.
9. C. Markert for the STAR Collaboration, SQM2001, *J. Phys. G* (2002) at press.
10. Z. Xu for the STAR Collaboration, *Nucl. Phys. A* **698** (2002) 607.
11. Particle Data Group, *Eur. Phys. J. C* **3** (1998).
12. P. Braun-Munzinger, D. Magestro, K. Redlich and J. Stachel, *Phys. Lett. B* **518** (2001) 41.
13. G. Torrieri and J. Rafelski, hep-ph/0112195, SQM2001, *J. Phys. G* (2002) at press.
14. J. Rafelski, J. Letessier and G. Torrieri, *Phys. Rev. C* **64** (2001) 054907.
15. G. Torrieri and J. Rafelski, *Phys. Lett. B* **509**, 239 (2001).
16. K.H. Ackermann, *et al.*, *Nucl. Phys. A* **661** (1999) 681.
17. S.V. Afanasiev, *et al.*, *Nucl. Instr. Meth. A* **430** (1999) 210.
18. For a more detailed discussion of experimental methods see contributions of J. Harris, and of K. Safarik in this volume.
19. J. Aichelin, G. Torrieri, and F. Gastineau, this volume.
20. M.F.M. Lutz and C.L. Korpa, nucl-th/0105067.
21. M.F.M. Lutz, E.E. Kolomeitsev and C.L. Korpa, SQM2001, *J. Phys. G* (2002) at press.
22. M. Gaździcki, M.I. Gorenstein, *Acta Phys. Polon. B* **30** (1999) 2705.
23. J. Canter *et al.*, *Phys. Rev. D* **20** (1979) 1029.
24. H. Albrecht *et al.*, *Z. Phys. C* **61** (1994) 1.
25. M. Aguilar-Benitz *et al.*, *Z. Phys. C* **50** (1991) 405.
26. M. Derrick *et al.*, *Phys. Lett. B* **158** (1985) 519.
27. D. Drijard *et al.*, *Z. Phys. C* **9** (1981) 293.
28. T. Akesson *et al.*, *Nucl. Phys. B* **203** (1982) 27.
29. A. Mischke for the NA49 Collaboration, SQM2001 *J. Phys. G* (2002) at press.
30. K. Abe *et al.*, *Phys. Rev. D* **59** (1990) 052001.
31. Y.J. Pei, *Z. Phys. C* **72** (1996) 39.
32. P.V. Chliapnikov, *Phys. Lett. B* **470** (1999) 263.
33. J. Aichelin, *Phys. Lett. B* **530** (2002) 81.
34. M. Bleicher private communication.
35. F. Becattini, M. Gaździcki, J. Sollfrank, *Eur. Phys. J. C* **5** (1998) 143.
36. F. Becattini, SQM2001, *J. Phys. G* (2002) at press.
37. S. Soff *et al.*, *J. Phys. G* **27** (2001) 449.
38. G. Torrieri and J. Rafelski, *Phys. Lett. B* **509** (2001) 239.
39. G. Torrieri and J. Rafelski, SQM2001, *J. Phys. G* (2002) at press.
40. F. Cooper and G. Frye, *Phys. Rev. D* **10** (1974) 186.
41. K. A. Bugaev, *Nucl. Phys. A* **606** (1996) 559.
42. C. Anderlik *et al.*, *Phys. Rev. C* **59** (1999) 3309.
43. M.A.C. Lamont, SQM2001, *J. Phys. G* (2002) at press.
44. E. Schnedermann, J. Sollfrank and U. Heinz NATO ASI series B, Physics vol. **303** (1995) 175.
45. E. Byckling and K. Kajantie, *Particle Kinematics*, Wiley (1973).
46. R. Kleiss, W.J. Stirling, *Nucl. Phys. B*, **385** (1992) 413.
47. A. Baldini, *et al* (eds), *Total cross-sections for reactions of high energy particles* Landolt-Börnstein numerical data and functional relationships in science and technology Springer (1990).
48. B.R. Martin, D. Morgan and G. Shaw, *Pion-Pion Interactions in Particle Physics* Academic Press, (New York 1976).
49. B. Muller, remarks in discussion session at this meeting.
50. R. Eisberg and R. Resnick, *Quantum physics of atoms, molecules, nuclei, and particles*, Wiley (1985).
51. A. Ruark and H. Urey, *Atoms, molecules, and quanta* McGraw-Hill (1964).